Supporting Information

Fe(TCNQ)₂ nanorod arrays: an efficient electrocatalyst for electrochemical ammonia synthesis *via* nitrate reduction reaction

Nilmadhab Mukherjee[1], Ashadul Adalder[1], Narad Barman[2], Ranjit Thapa[2], Rajashri Urkude[3], Biplab Ghosh[3] and Uttam Kumar Ghorai[1]*

[1]Department of Industrial Chemistry & Applied Chemistry, Swami Vivekananda Research Centre, Ramakrishna Mission Vidyamandira, Belur Math, Howrah - 711202, India

[2]Department of Physics and Centre for Computational and Integrative Sciences, SRM University – AP, Amaravati 522240, Andhra Pradesh, India

[3]Beamline Development & Application Section, Bhabha Atomic Research Center, Trombay, Mumbai 400085, India

* E-mail: uttam.indchem@vidyamandira.ac.in

SI 1: Determination of ammonia using UV-vis spectrophotometer:

By employing a UV-vis spectrophotometer and the indophenol blue technique, ammonia was measured. To create a 1M sodium hydroxide (Merck) solution that would serve as the colouring solution, 5 wt% trisodium citrate dihydrate (Merck) and 5 wt% salicylic acid (Merck) were added. As an oxidising agent, 0.05 M sodium hypochlorite (Merck) solution was utilised. Catalyst solution contained 3.34 mmol of sodium nitroprusside dihydrate (Loba Chemie). After NO_3RR electrolysis, 2 mL of colouring solution, 1 mL of oxidising solution, and 0.2 mL of catalyst solution were combined with 2 mL of electrolyte solution after certain dilution. After incubating the resultant solution at room temperature for two hours, it was spectrophotometrically examined. Indophenol was found to be present in the combination solution according to the maximum absorbance at ~655 nm. After incubating the combination solution at room temperature for two hours, it was examined in a UV-vis spectrophotometer. The production of indophenol was verified by the maximum absorbance peak at ~655 nm. With concentrations ranging from 0.0 to 1.0 (µg/mL) in 0.1M Na_2SO_4 solution, ammonium ion concentration was employed for calibration using ammonium chloride (Merck). Following calibration, the fitting curve from (y=0.1282x + 0.0425, R^2 = 0.999) showed an optimised linear relationship of absorbance with ammonia concentration.

SI 2: Nafion 117 membrane treatment:

The membrane was prepared for the test by boiling it in distilled water for an hour and then treated it with a 5% H_2O_2 aqueous solution at 80 °C for an hour. The membrane was once again treated in 0.5 M H_2SO_4 for 2 hours at 80 °C before being heated in distilled water for another 6 hours.

SI 3: Isotope labelling experiments by ¹H NMR method:

An isotope-labelled tracer electrochemical experiment utilising a solution of $Na^{15}NO_3$ (98 atom% ^{15}N Sigma-Aldrich Co. as the nitrogenous source) as the nitrogenous source was used to verify the electrochemically produced $^{15}NH_3$ from $^{15}NO_3^-$. After an hour of electrocatalytic nitrate reduction, the $^{15}NH_4^+$ produced in the electrolyte solution was assessed using ^1H-NMR (600 MHz) spectroscopy. Before the NMR analysis, the NMR sample was prepared by mixing 0.4 mL electrolyte (acidified with 0.05 M H_2SO_4) with 0.1 mL D_2O as an internal standard solvent for NMR.

SI4: Formula for the ammonia yield rate and Faradaic efficiency calculation

The following equation was used to calculate the rate of ammonia formation:

$$\text{Rate of NH}_3 = \frac{\left(C_{NH_3} \text{ x V}\right)}{\text{t x S}}$$

Where V is the volume of the NO_3RR electrolyte, t is the reduction period, S is the catalytic surface area, and C_{NH_3} is the concentration of ammonia after the NO_3RR.

According to the following equation, the faradaic efficiency may be determined:

$$\text{FE (\%)} = \frac{\left(8 \text{ x F x } C_{NH_3} \text{ x V}\right)}{\text{M x Q}} \text{ x 100\%}$$

F is the Faraday Constant, which is 96485.33 C mol^{-1}. C_{NH_3} is the amount of ammonia left over after NO_3RR, V is the volume of NO_3RR electrolyte, Q denotes the total charge that travelled through the electrode during reduction, and M denotes the molar mass of ammonia.

The following equation may be used to determine the number of turnovers and turnover frequency:[1]

$$\text{TOF} = \frac{\left(\text{Yield rate, } \mu g \text{ } h^{-1} cm^{-2}\right) \text{ x Geometric surface area x } N_A}{\text{Surface active sites x Molar mass of ammonia x ECSA}}$$

$$\text{Surface sites} = \left(\frac{\text{Atoms per unit cell}}{\text{Volume per unit cell}} \right)^{\frac{2}{3}}$$

$Fe(TCNQ)_2$ is a monoclinic system.[2]

Volume per unit cell = 1051.974 Å^3

So, $Fe(TCNQ)_2$ system the surface sites is 1.53×10^{14} cm^{-2}.

ECSA stands for electrochemical active surface area (252 cm^2), while N_A is the Avogadro constant (6.023×10^{23} mol^{-1})

Geometric surface area: 0.9 cm^2

Yield rate: 11351.6 μg h^{-1} cm^{-2}

Molar mass of ammonia: 17 g/mol

$$\text{TOF} = \frac{\left(11351.6,\ \mu g\ h^{-1} cm^{-2}\right) \times \left(0.9,\ cm^2\right) \times \left(6.023 \times 10^{23},\ mol^{-1}\right)}{\left(1.53 \times 10^{14},\ cm^{-2}\right) \times \left(17,\ g\ mol^{-1}\right) \times \left(252,\ cm^2\right)}$$

$$\text{TOF} = \frac{\left(11351.6 \times 10^{-6},\ g\ cm^{-2}\right) \times \left(0.9,\ cm^2\right) \times \left(6.023 \times 10^{23},\ mol^{-1}\right)}{\left(1.53 \times 10^{14},\ cm^{-2}\right) \times \left(17,\ g\ mol^{-1}\right) \times \left(252,\ cm^2\right) \times \left(3600,\ s\right)}$$

TOF = 2.6 s^{-1}

S15: Computational details:

In this work, we have used density functional theory based VASP code as a computational tool to perform the required simulations. Because of periodic nature of the system considered here plane wave basis set is incorporated and plane waves are expanded within a maximum kinetic energy cut-off of 520 eV^3. In case of total energy calculations, we have introduced two types of convergence criteria for ionic and electronic relaxations, one is energy convergence which is set to be $1E^{-6}$ eV and another one is ionic force convergence, set to be -0.01 eV/Å. To illustrate the effects of exchange and correlation forces among electrons, many approximations method are reported, here we have applied General Gradient Approximation of PBE functional[4]. Projected Augmented Wave method has been used to demonstrate the

pseudo potential based interaction between core and valence electrons, created by freezing the core part. Long range weak Van der Waal forces among atoms in the given system are managed by employing Grimme DFT-D2 dispersion scheme[5]. To sample the Brillouin zone of the reporting system in k-space, we have applied popular k-point sampling method, Monk-Horst grid method, with 5 X 5 X 1 k-points for structural optimization and 9 X 9 X 1 k-points assumed for DOS calculations.
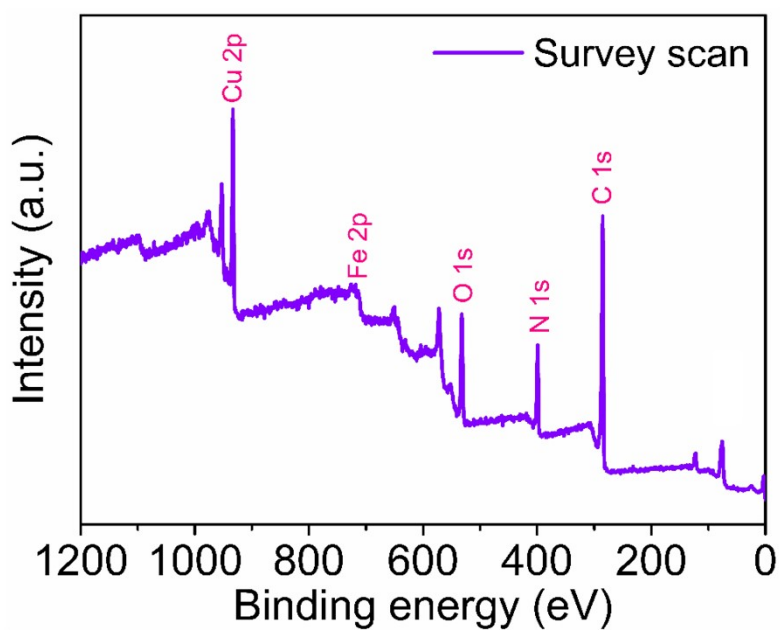

Fig. S1: XPS survey scan of Fe(TCNQ)$_2$/CF (before electrolysis)
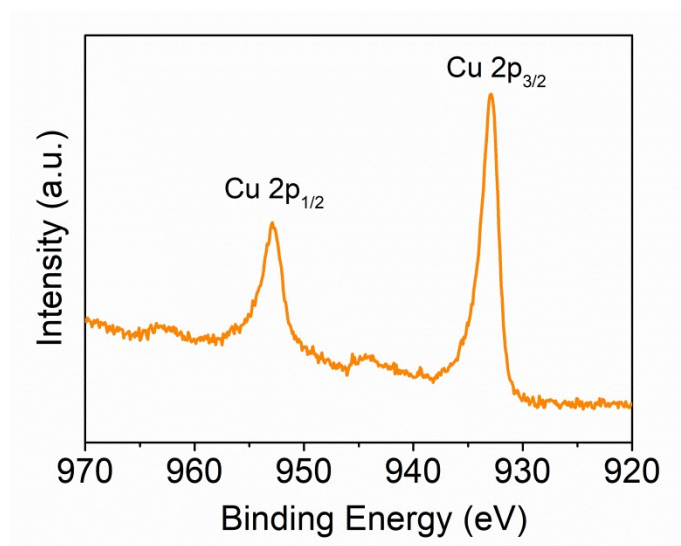
Fig. S2: High resolution XPS spectrum of Cu 2p in Fe(TCNQ)$_2$/CF
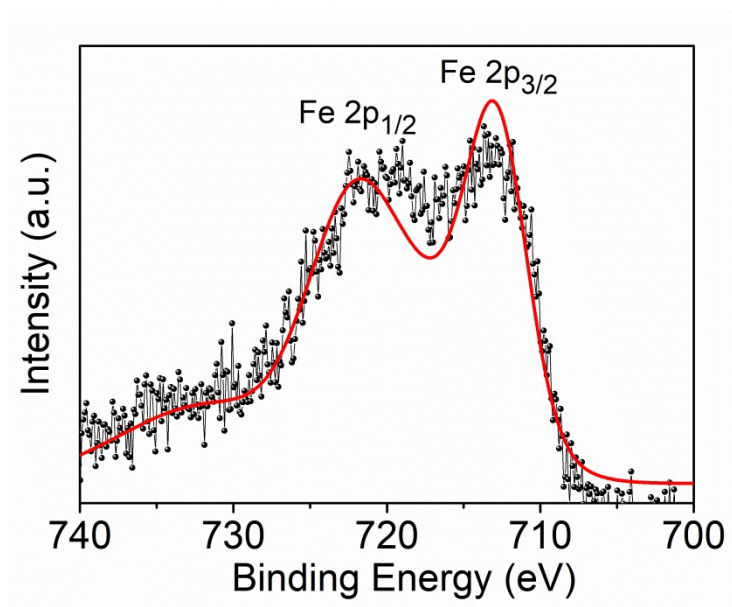
Fig. S3: High resolution XPS spectrum of Fe 2p of Fe(TCNQ)$_2$/CF (after electrolysis)
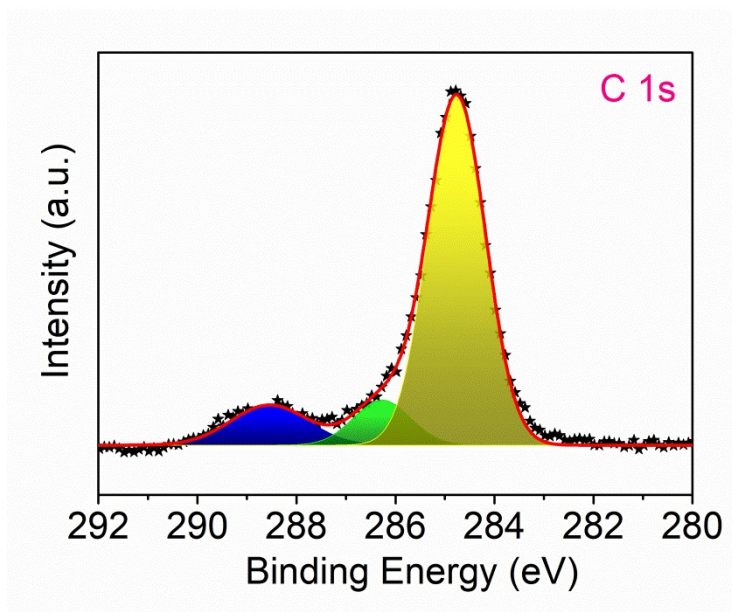
Fig. S4: High resolution XPS spectrum of C 1s of $Fe(TCNQ)_2$/CF (after electrolysis)
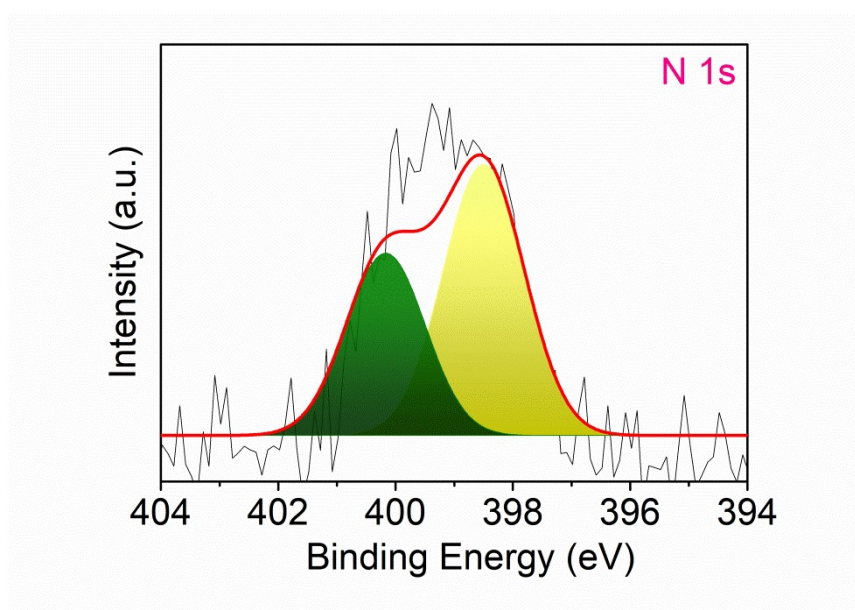
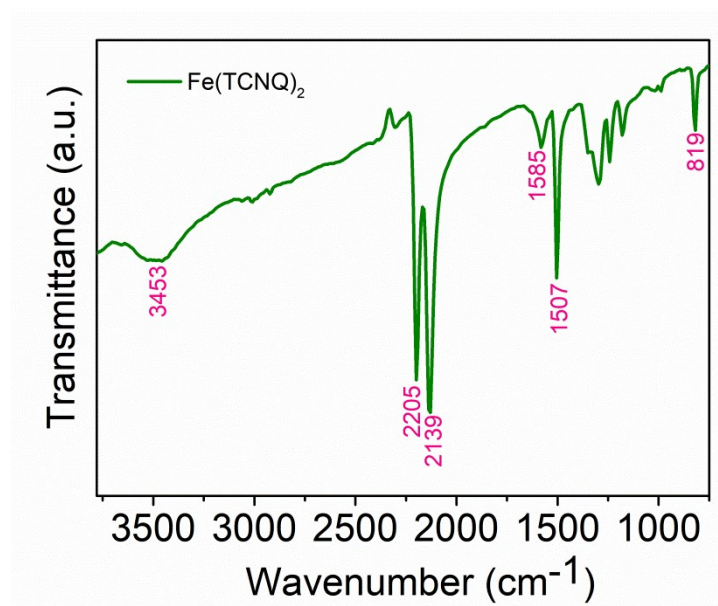**Fig. S5**: High resolution XPS spectrum of N 1s of $Fe(TCNQ)_2$/CF (after electrolysis)

Fig. S6: FTIR spectrum of Fe(TCNQ)$_2$

The production of the Fe(TCNQ)$_2$ is supported by the FT-IR findings. Resolved bands at 2139, and 2205 cm^{-1}, which are in agreement with the C≡N band, corresponds to the existence of TCNQ. Simultaneously, the C=C and C-H bending bands of TCNQ are indicated by two typical peaks at 1502 and 816 cm^{-1}. A wide band at 3460 cm^{-1} and a faint peak at 1586 cm^{-1} show coordinated water molecules are present in the post-synthetic material.[6,7]
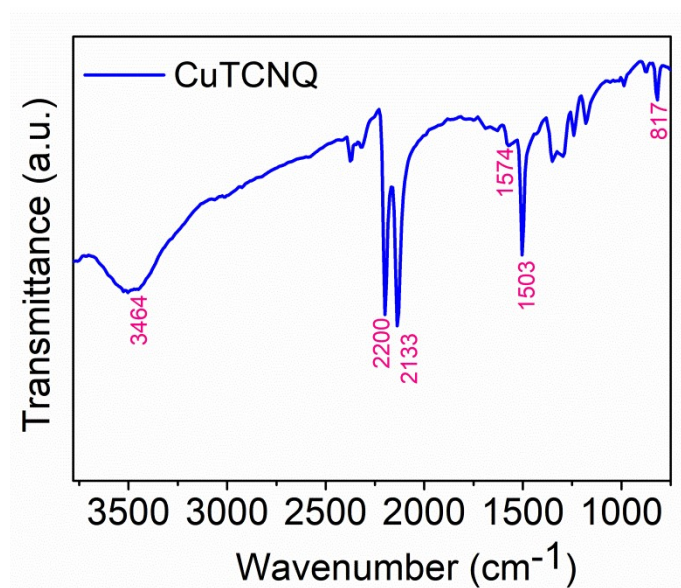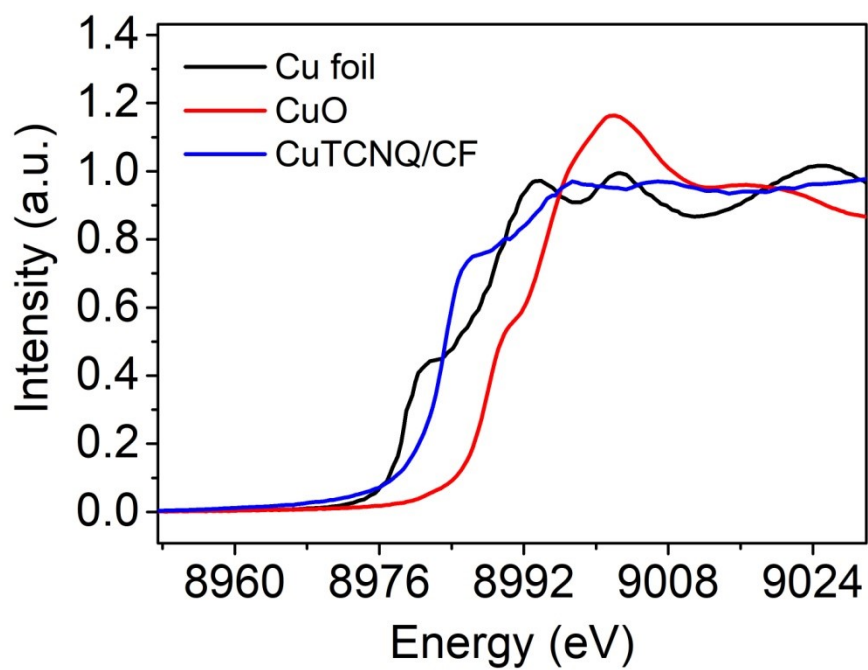

Fig. S7: FTIR spectrum of CuTCNQ

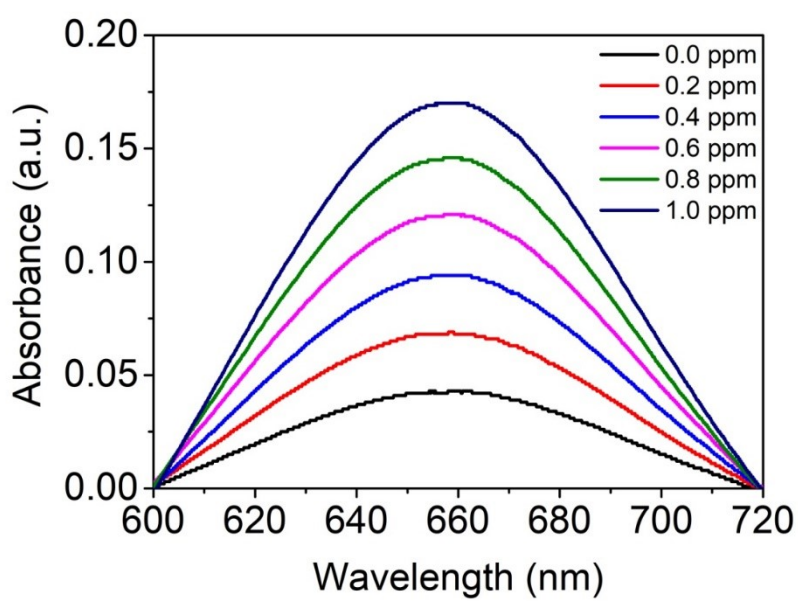**Fig. S8**: XANES spectra of Cu foil, CuO and CuTCNQ/CF

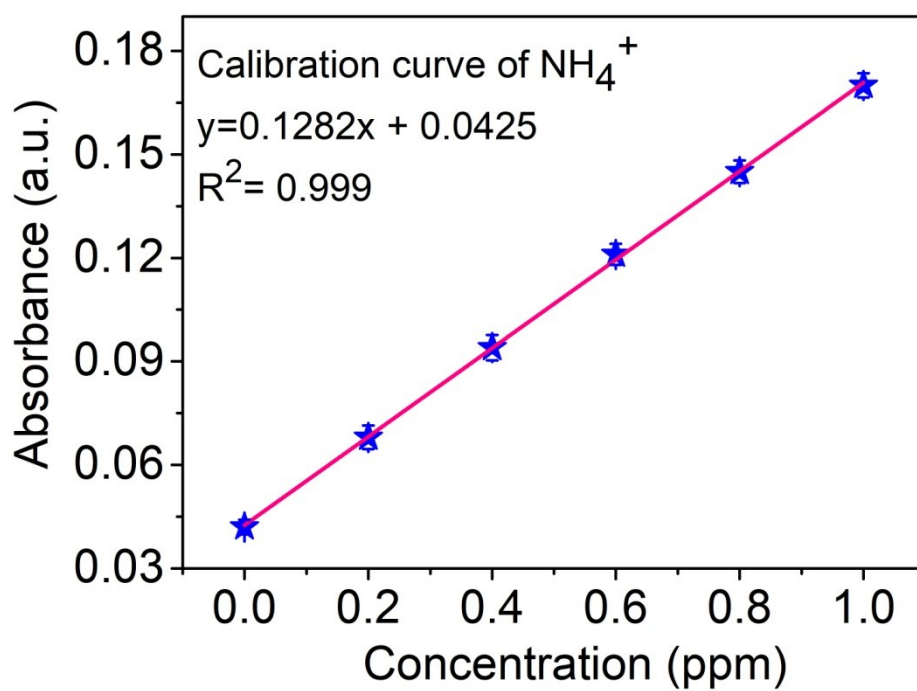**Fig. S9**: Calibration of ammonium solutions with known concentrations

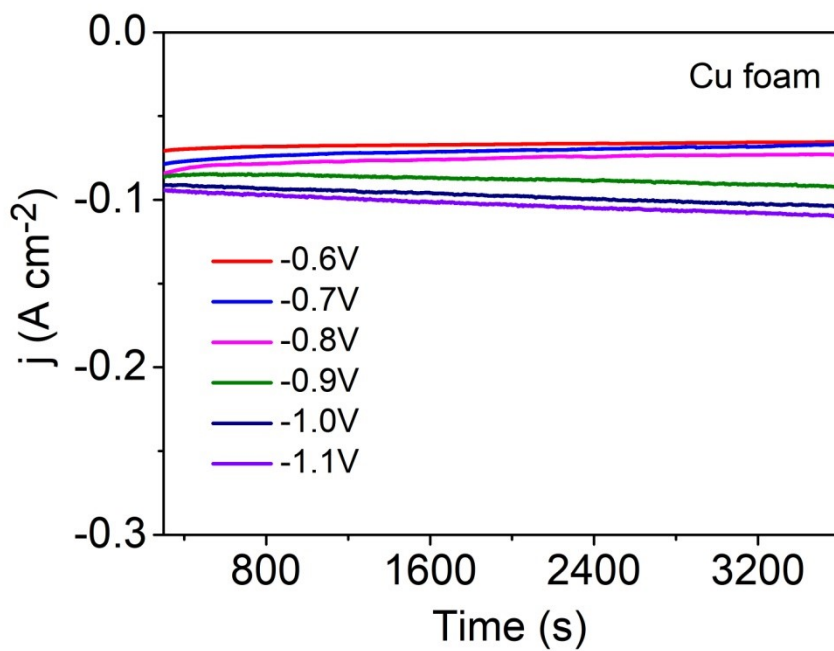**Fig. S10**: The standard curve of absorbance as a function of NH_4^+ concentration
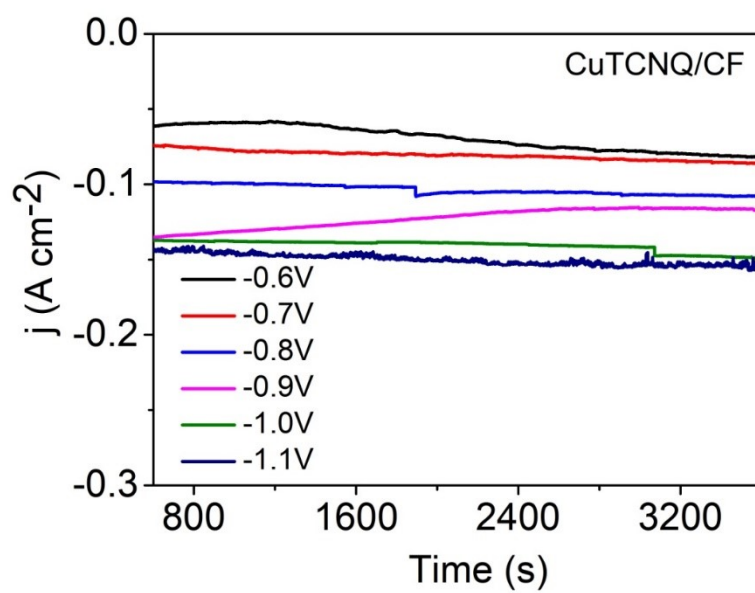

Fig. S11: The j-t curves of NO_3RR test for Cu foam

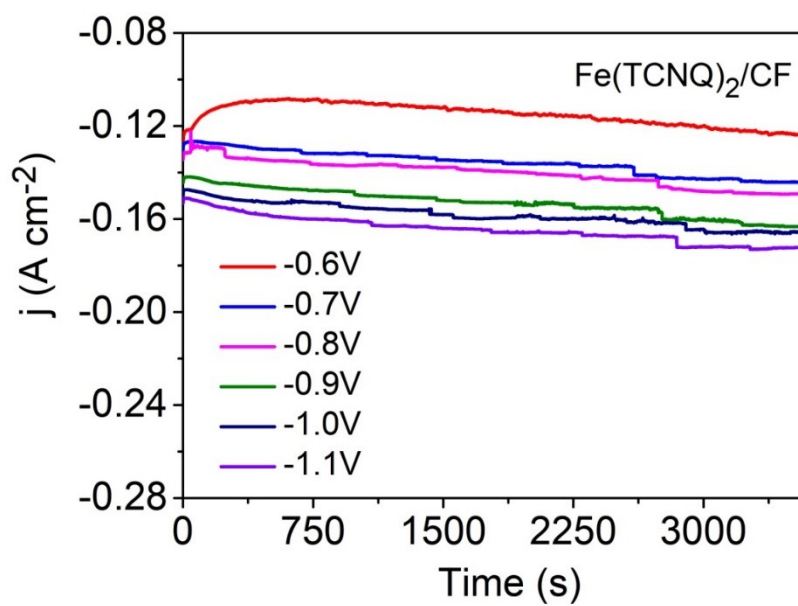**Fig. S12**: The j-t curves of NO$_3$RR test for CuTCNQ/CF

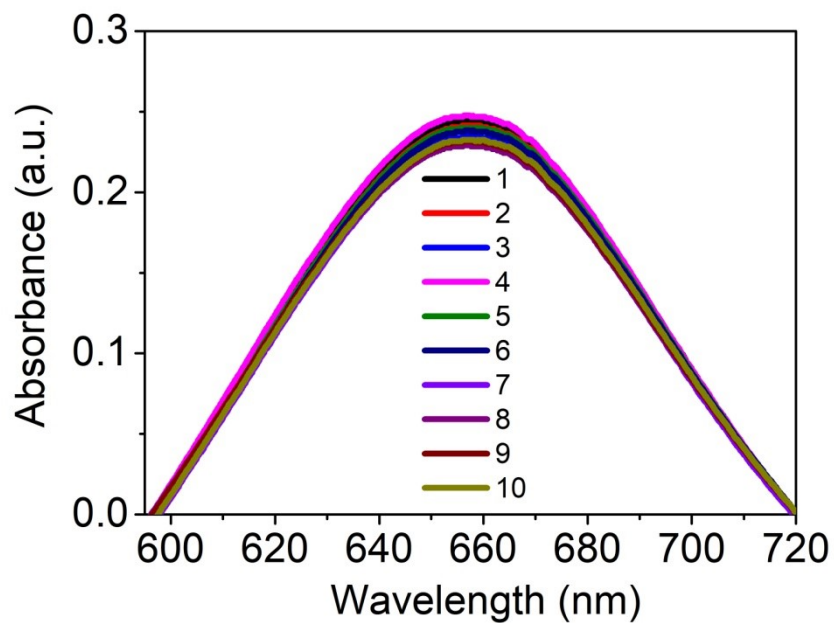**Fig. S13**: The j-t curves of NO$_3$RR test for Fe(TCNQ)$_2$/CF

Fig. S14: The cycling tests of Fe(TCNQ)$_2$/CF for reduction tests by UV–vis spectroscopy

Fig. S15: CV curves at various scan rates (20, 40, 60, 80 and 100 mV s^{-1}) for Cu foam

Fig. S16: The differences (δj/2) between capacitive currents at the center of selected potential window as a function of scan rate for Cu foam
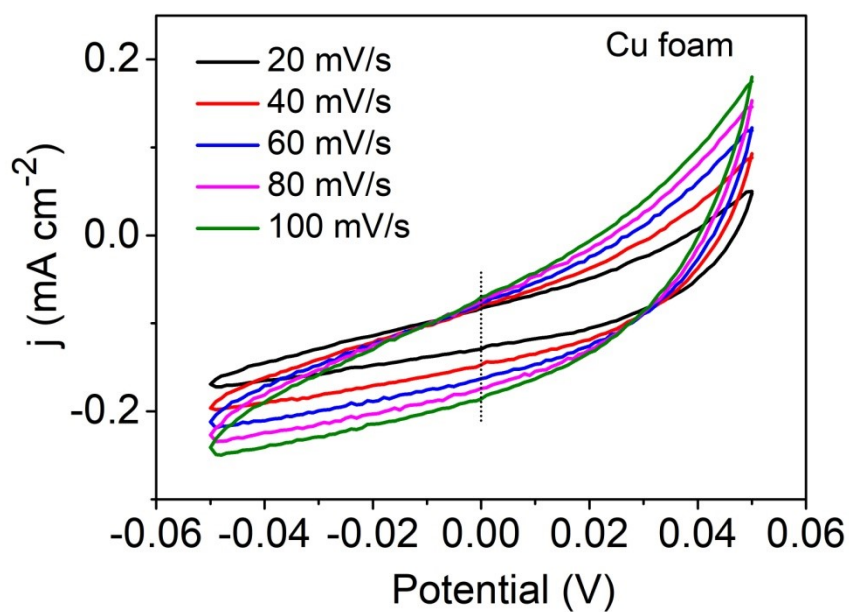

Fig. S17: CV curves at various scan rates (20, 40, 60, 80 and 100 mV s^{-1}) for CuTCNQ/CF

Fig. S18: The differences ($\delta j/2$) between capacitive currents at the center of selected potential window as a function of scan rate for CuTCNQ/CF

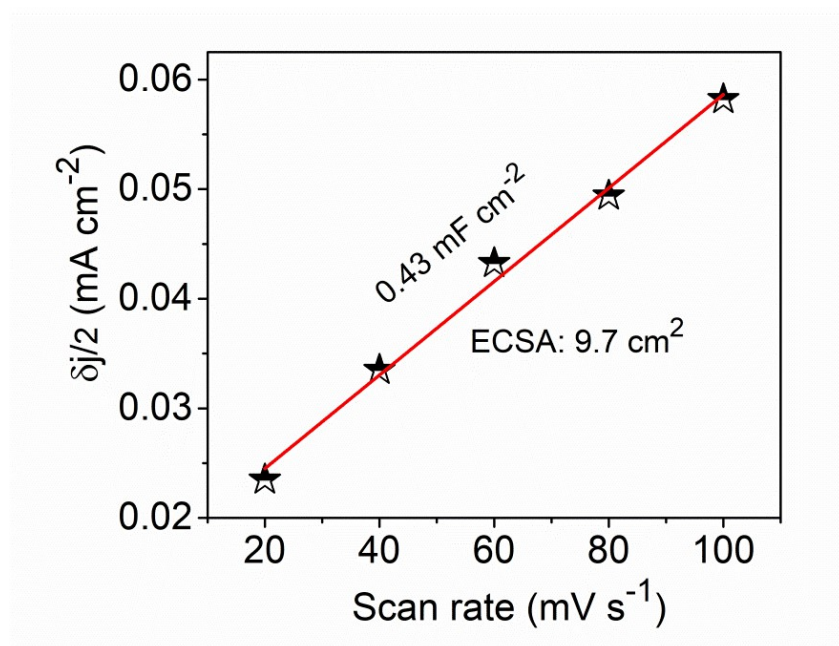**Fig. S19**: CV curves at various scan rates (20, 40, 60, 80 and 100 mV s^{-1}) for Fe(TCNQ)$_2$/CF

Fig. S20: The differences (δj/2) between capacitive currents at the center of selected potential window as a function of scan rate for Fe(TCNQ)$_2$/CF
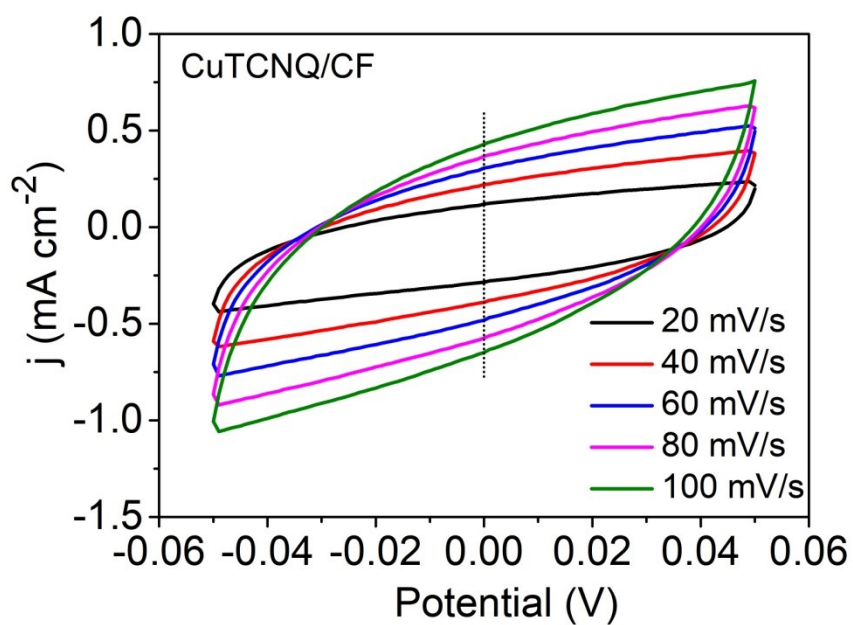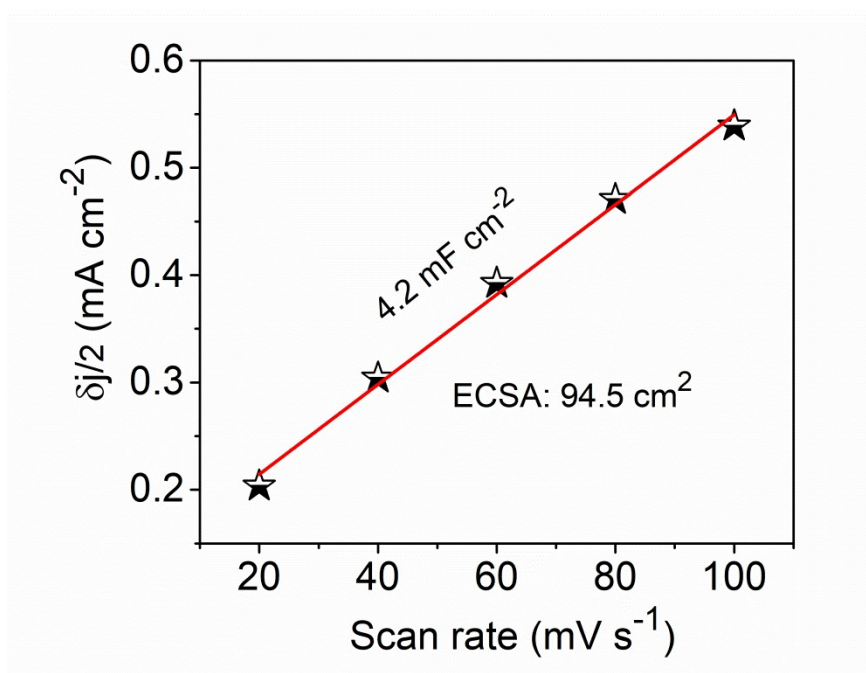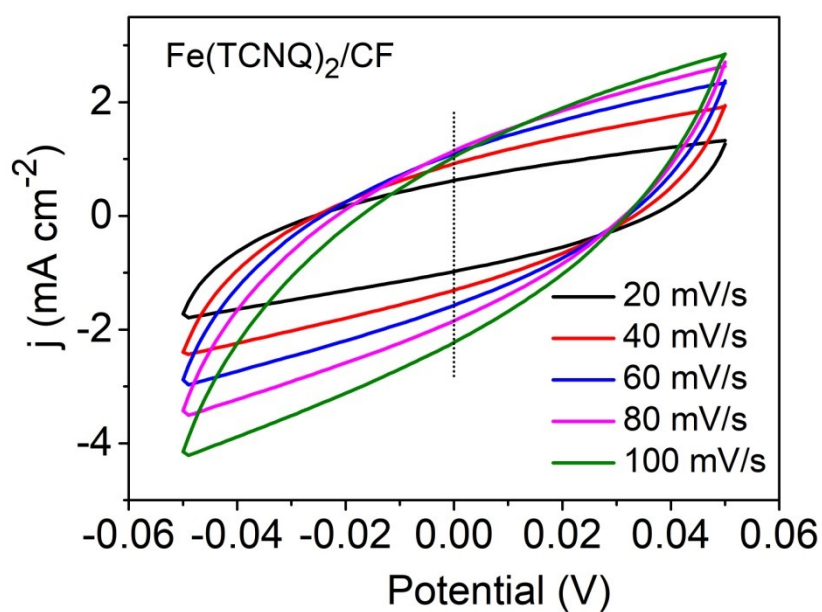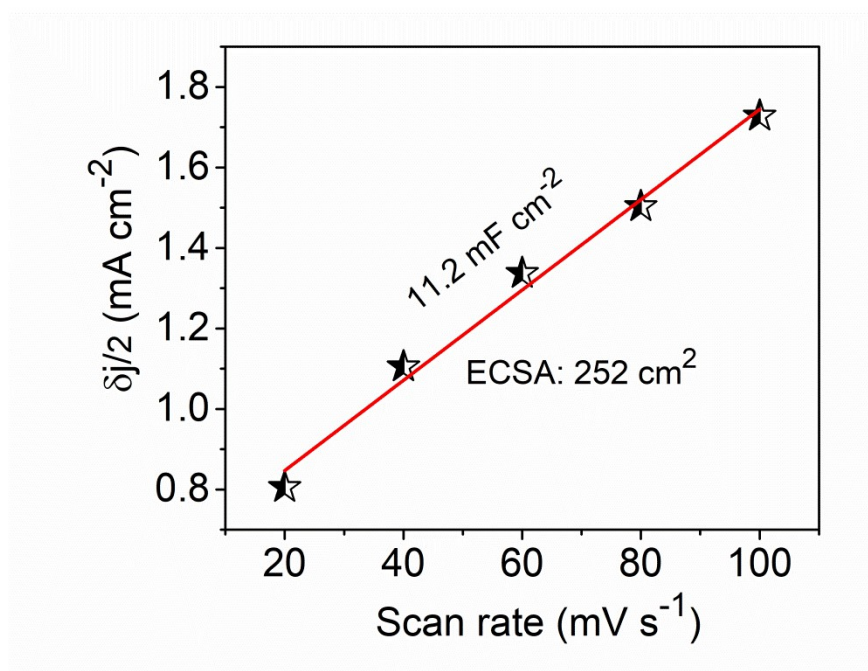
By dividing the measured C_{dl} by the capacitance of the generally used specific capacitance for the catalytic system over a unit surface area, the electrochemically surface area (ECSA) was computed, and specific capacitance (C_s) value is taken as 40 µF/cm^2.[8]

We have calculated the electrochemical active surface area (ECSA):

ECSA = $R_f \times$ S

Where R_f stands for roughness factor of the working electrode:

R_f = ($C_{dl} \div$ Cs) = ($C_{dl} \div$ 40 µF cm^{-2})

S represents the geometric surface area of the electrode

The geometric surface area of the working electrode = 0.9 cm^2

Calculation:

For Fe(TCNQ)$_2$/CF,

C_{dl} = 11.2 mF cm^{-2}, so R_f = { (11.2 × 1000) ÷ 40 } = 280

ECSA [Fe(TCNQ)$_2$/CF] = 280 × 0.9 = 252 cm^2

For CuTCNQ/CF,

C_{dl} = 4.2 mF cm^{-2}, so R_f = { (4.2 × 1000) ÷ 40 } = 105

ECSA [CuTCNQ/CF] = 105 × 0.9 = 94.5 cm^2
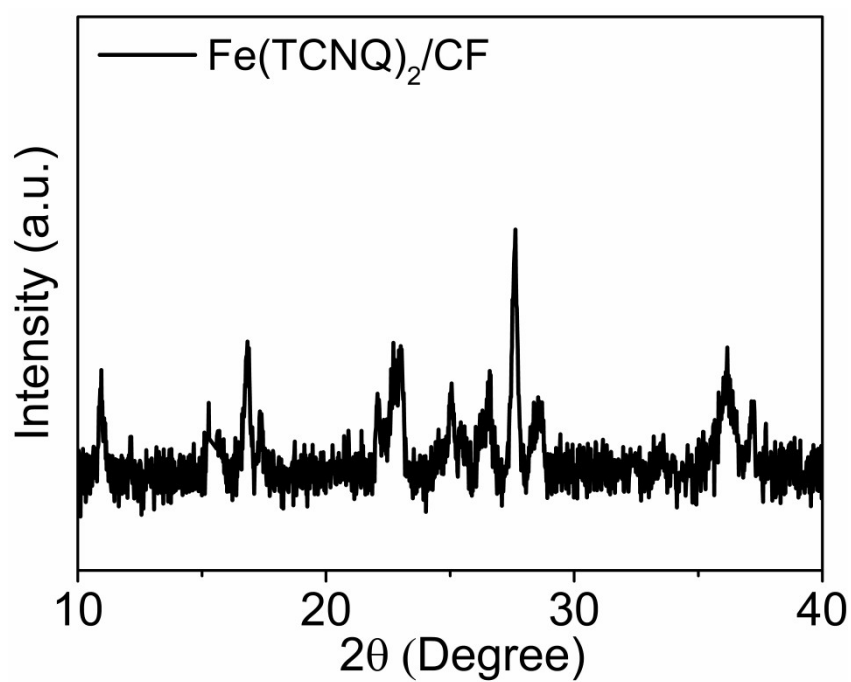
Fig. S21: XRD pattern for Fe(TCNQ)$_2$/CF (after electrolysis)

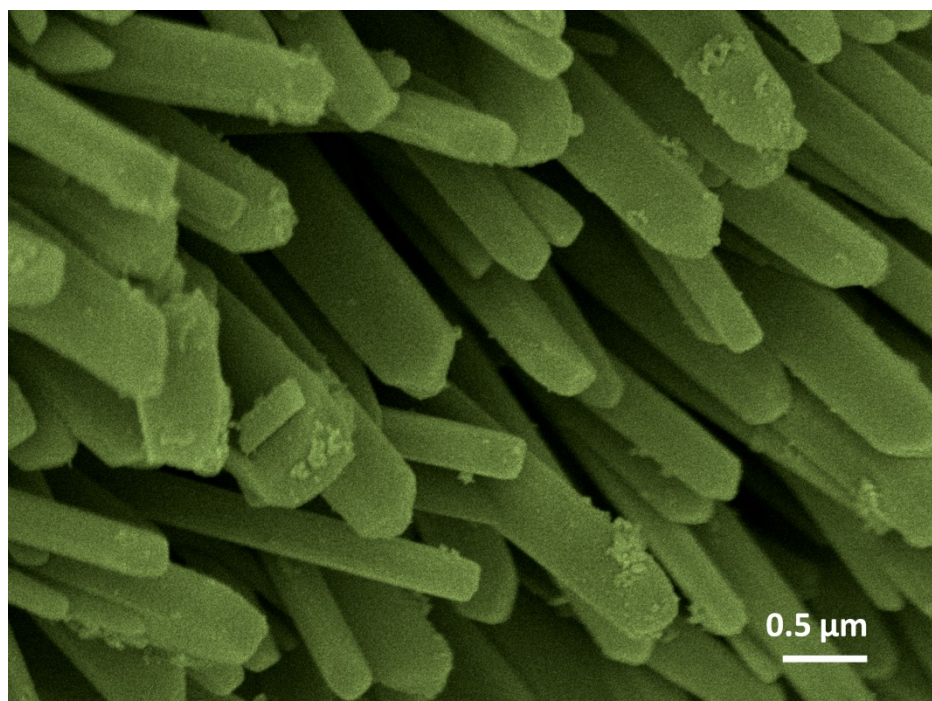**Fig. S22:** FESEM image of Fe(TCNQ)$_2$/CF (after electrolysis)
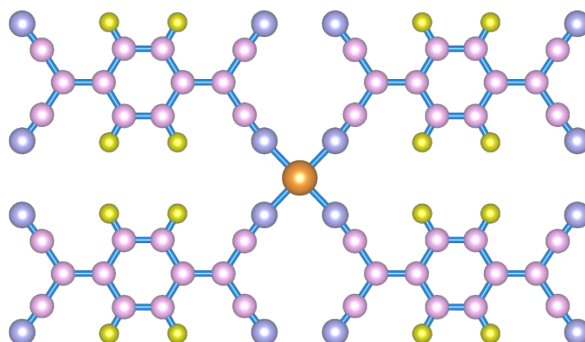
Fig. S23: Optimized model structure of Fe-TCNQ
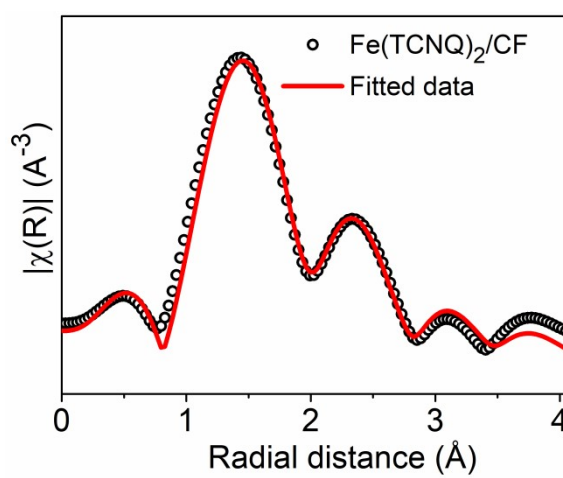
Fig. S24: Experimental χ(R) vs R data of Fe(TCNQ)$_2$/CF measured at the Fe K-edge with fitting

Table S1: EXAFS fitting parameters at the Fe K-edge for sample

Sample	Shell	N	R (Å)	σ^2 (Å^2)	ΔE_0 (eV)	R factor
Fe(TCNQ)$_2$/CF	Fe-N	4	2.014 +/- 0.015	0.002 +/- 0.001	-0.98 +/- 2.08	0.0157

N: coordination number; R: bond distance; σ^2: Debye-Waller factor; ΔE_0: the inner potential correction. R factor: goodness of fit. S_0^2 was set as 0.754.

Table-S2

Adsorbed Molecule	ZPE (eV)	TS (eV)	ZPE-TS (eV)
NO$_3$	0.396038	0.219128	0.17691
NO$_3$H	0.695769	0.367404	0.328365
NO$_2$	0.272663	0.154073	0.11859
NO$_2$H	0.59261	0.216491	0.376119
NO	0.185625	0.157299	0.028327
NHO	0.4512	0.127954	0.323246
NHOH	0.801001	0.166158	0.634843
NH$_2$OH	1.113142	0.174641	0.938502
NH$_2$	0.680361	0.092387	0.587973
NH$_3$	1.000728	0.153737	0.846991
N	0.081048	0.051131	0.029917
NH	0.32335	0.09107	0.23228

Free Molecule	Total Energy (eV)
NO_3	-23.745
N_2	-16.63
H_2O	-14.25
H	-3.45
NH_3	-19.24

Table-S4: A comparison table of performance NO_3RR with other previously reported catalysts

Catalyst	Electrolyte	Potential (V)	Yield rate	FE (%)	Reference
Fe SAC	$K_2SO_4/$ KNO_3	−0.66 V	0.46 mmol h^{-1} cm^{-2}	~ 75%	9
Au–Cu NWs/CF	0.1 M Na_2SO_4 + 10.0 mM KNO_3	−1.05 V	5336.0 ± 159.2 mg h^{-1} cm^{-2}	84.1 ± 1.0%	10
Cu_3Fe	0.1 M Na_2SO_4 + 100 ppm NO_3^-	−0.7 V	--	81.1%	11
Co_3O_4@NiO HNTs	0.5 mol L^{-1} Na_2SO_4 + 200 ppm $NaNO_3$	−0.70 V	6.93 mmol h^{-1} g^{-1}	--	12
Fe-N/P-C	0.1 M KOH + 0.1 M KNO_3	−0.8 V	17980 µg h^{-1} mg_{cat}^{-1}	90.3%	13
Indium in S doped graphene	1 M KOH + 0.1 M KNO_3	−0.5 V	220 mmol g^{-1}_{cat} h^{-1}	75%	14
PTCDA/O-Cu	0.1 M PBS (500 ppm NO_3^-)	−0.40 V	436 ± 85 µg h^{-1} cm^{-2}	85.9%	15
Cu_3P NA/CF	0.1 M PBS (0.1 M NO_3^-)	−0.50 V	1626.6 ± 36.1 µg h^{-1} cm^{-2}	91.2± 2.5%	16
Fe-PPy SACs	0.1 M KOH + 0.1 M KNO_3	−0.7 V	2.75 mg_{NH3} h^{-1} cm^{-2}	100%	17
Cu SAC	0.1 M KOH + 0.1 M KNO_3	−1.0 V	4.5 mg cm^{-2} h^{-1}	84.7%	18
Fe@Fe_2O_3	50 ppm $NaNO_3$ + 0.1M Na_2SO_4	−0.645 V	1505.9 µg h^{-1} cm^{-2}	85.2 ± 0.6%	19
Fe(TCNQ)₂/CF	**0.2 M $NaNO_3$ + 0.1 M Na_2SO_4**	**−1.1 V**	**11351.6 µg h^{-1} cm^{-2}**	**85.2%**	**This work**

References:

1   T. Xu, D. Ma, T. Li, L. Yue, Y. Luo, S. Lu, X. Shi, A. M. Asiri, C. Yang and X. Sun, *Chem. Commun.*, 2020, **56**, 14031–14034.

2   P. J. Spellane, L. V. Interrante, R. K. Kullnig and F. S. Tham, *Inorg. Chem.*, 1989, **28**, 1587–1590.

3   G. Kresse and J. Furthmüller, *Comput. Mater. Sci.*, 1996, **6**, 15–50.

4   J. P. Perdew, K. Burke and M. Ernzerhof, *Phys. Rev. Lett.*, 1996, **77**, 3865.

5   S. Grimme, *J. Comput. Chem.*, 2006, **27**, 1787–1799.

6   X. Guo, S. Zhu, R. M. Kong, X. Zhang and F. Qu, *ACS Sustain. Chem. Eng.*, 2018, **6**, 1545–1549.

7   M. Xie, X. Xiong, L. Yang, X. Shi, A. M. Asiri and X. Sun, *Chem. Commun.*, 2018, **54**, 2300–2303.

8   S. Paul, S. Sarkar, D. Dolui, D. Sarkar, M. Robert and U. K. Ghorai, *Dalt. Trans.*, 2023, **52**, 15360–15364.

9   Z. Y. Wu, M. Karamad, X. Yong, Q. Huang, D. A. Cullen, P. Zhu, C. Xia, Q. Xiao, M. Shakouri, F. Y. Chen, J. Y. (Timothy) Kim, Y. Xia, K. Heck, Y. Hu, M. S. Wong, Q. Li, I. Gates, S. Siahrostami and H. Wang, *Nat. Commun.*, 2021, **12**, 1–10.

10   Y. Zha, M. Liu, J. Wang, J. Feng, D. Li, D. Zhao, S. Zhang and T. Shi, *RSC Adv.*, 2023, **13**, 9839–9844.

11   Z. Tang, Z. Bai, X. Li, L. Ding, B. Zhang and X. Chang, *Processes*, 2022, **10**, 751.

12   Y. Wang, C. Liu, B. Zhang and Y. Yu, *Sci. China Mater.*, 2020, **63**, 2530–2538.

13   J. Xu, S. Zhang, H. Liu, S. Liu, Y. Yuan, Y. Meng, M. Wang, C. Shen, Q. Peng, J. Chen, X. Wang, L. Song, K. Li and W. Chen, *Angew. Chemie Int. Ed.*, 2023, **62**, e202308044.

14   F. Lei, W. Xu, J. Yu, K. Li, J. Xie, P. Hao, G. Cui and B. Tang, *Chem. Eng. J.*, 2021, **426**, 131317.

15   G. F. Chen, Y. Yuan, H. Jiang, S. Y. Ren, L. X. Ding, L. Ma, T. Wu, J. Lu and H. Wang, *Nat. Energy*, 2020, **5**, 605–613.

16   J. Liang, B. Deng, Q. Liu, G. Wen, Q. Liu, T. Li, Y. Luo, A. A. Alshehri, K. A. Alzahrani, D. Ma and X. Sun, *Green Chem.*, 2021, **23**, 5487–5493.

17   P. Li, Z. Jin, Z. Fang and G. Yu, *Energy Environ. Sci.*, 2021, **14**, 3522–3531.

18   J. Yang, H. Qi, A. Li, X. Liu, X. Yang, S. Zhang, Q. Zhao, Q. Jiang, Y. Su, L. Zhang, J. F. Li, Z. Q. Tian, W. Liu, A. Wang and T. Zhang, *J. Am. Chem. Soc.*, 2022, **144**, 12062–12071.

19   S. Zhang, M. Li, J. Li, Q. Song and X. Liu, *Proc. Natl. Acad. Sci. U. S. A.*, 2022, **119**, e2115504119.